Optical Spectroscopy of Potassium-Doped Argon Clusters. Experiments and Quantum-Chemistry Calculations[†]

Johann Nagl,* Andreas W. Hauser, Gerald Auböck, Carlo Callegari, and Wolfgang E. Ernst

Institute of Experimental Physics, Graz University of Technology, Petersgasse 16, A-8010 Graz, Austria/EU

Received: July 27, 2007; In Final Form: August 31, 2007

Rare-gas clusters produced in a supersonic expansion into vacuum are doped with alkali-metal atoms using the pickup technique. We give here a detailed description of our experimental apparatus, which is suitable for electronic spectroscopy of any desired gas clusters doped with low-temperature melting metals. Potassium-doped Ar clusters (average size $\bar{N} \approx 2000$) are investigated by beam-depletion (BD) spectroscopy as well as laser-induced fluorescence (LIF) spectroscopy. The observed BD spectra are strong and exhibit several broad peaks within the scan range of the Ti:sapphire excitation laser; only one weak band is observed instead in LIF spectra. This situation resembles the one previously observed for K-doped H_2 clusters [Callegari et al., *J. Phys. Chem. A* **1998**, *102*, 4952] where it was argued that fluorescence is either quenched or strongly red-shifted by the cluster. We investigate BD spectra as a function of the potassium vapor pressure in the pickup cell, and we perform an extensive analysis of the pickup process, necessary to separate the overlapping spectral contributions of different species. We tentatively assign parts of the spectra to the monomer, singlet dimer, and doublet trimer, of potassium residing on the surface of the cluster. To support our trimer assignment, we perform complete active space self-consistent field (CASSCF) calculations to determine the lowest 12 electronic spin-doublet states of free K_3. We find several candidate transitions in the region of interest. Although a definite assignment is not possible because the energy shifts due to the perturbation by the Ar cluster are not known, our theoretical and experimental data compare favorably with existing spectra, and with simulations, of the closely related Na_3-molecule, upon suitable scaling of its energy-level structure.

I. Introduction

Rare-gas clusters have been used in spectroscopy as a microscopic matrix,[1,2] drawing from the rich field of matrix isolation spectroscopy;[3,4] dopants may be the very object under investigation, or the probe of the cluster itself, because pure rare-gas clusters have no transitions in the visible.

Among all rare gases, argon clusters have a special place: van der Waals forces between Ar atoms are strong enough that only modest cooling is necessary to produce large clusters in a supersonic expansion, yet weak enough to result in a low cluster temperature, $T = 35 \pm 4$ K,[5] and in a weak perturbation of the spectra of dopants. Theoretical simulations too benefit from the weak, well-known interactions, which can be treated classically and, to a reasonably good approximation, as a sum of pair potentials.[6]

The dependence of the structure of Ar clusters on their size has been widely investigated. It is found that clusters smaller than 100 atoms are amorphous, then the icosahedral structure is prevalent up to a few thousand atoms, where it is superseded by a mixed hcp/fcc structure.[5,7,8] The clusters produced in a supersonic expansion are not monodisperse. Instead, their size N follows a log-normal distribution,[9] whose width and mean value are of the same order. Thus, one can expect doped clusters to yield inhomogeneous spectra, due to different cluster structures, or to different trapping geometries.

Dopants are attached onto a cluster by the "pickup" technique[1] where the cluster passes through a heatable cell kept at temperature T_c. The pickup cell contains the dopant species at a set vapor density ρ. Depending on the value of ρ, the clusters capture a certain mean number of atoms inside the cell, through collision. It is generally accepted that successive pickup events can be treated as independent, which results in a Poisson distribution of the number n of dopant species per cluster. Possible corrections are discussed in ref 10; note that for alkali-metal atoms on He droplets, a different description of the pickup process has been proposed,[11] in which successive pickup events are significantly correlated and a different distribution of n results.

The cluster dissipates the kinetic and binding energy of the captured species by evaporation of atoms. Because the energy to be dissipated is large, and because in general there is no reason to expect the existence of large barriers, one normally assumes that the energetically most favorable configuration is always formed. Exceptions occur for He droplets, where cooling is so fast that dopants end up in local minima, either because different spin multiplicities do not interconvert[12] or because long-range forces drive the system into that local minimum, which is easier to reach when a monomer component is added. The latter has been observed for chains of HCN[13] and HC-CCN,[14] CH_3OH tetramers,[15] and H_2O hexamers.[16]

As far as the final location of a single dopant is concerned, molecular dynamics (MD) simulations show[17] that it is strongly dependent on the properties of the clusters, as well as on the pickup process, possibly giving rise to metastable trapping sites whenever local melting of the cluster by collision is followed by rapid cooling. In such a case, it is hard to predict where on the cluster the dopant will be located. A simple criterion to decide on the most favorable location, based on extrapolation of MD results for a set of dopant molecules, has been proposed by Perera and Amar.[18] It is quantitative and appears to be reliable

Optical Spectroscopy of Potassium-Doped Ar Clusters

J. Phys. Chem. A, Vol. 111, No. 49, 2007 **12387**

for cases that are far from borderline. According to it, potassium, being much larger than argon and having a weaker interaction with Ar than Ar with itself, should definitely reside on the surface (see also section IIIC).

Many spectroscopic experiments have been performed on doped rare-gas clusters; the results are reviewed in several monographs covering broader themes in cluster science.[19−21] Ongoing fields of experimental research utilizing Ar clusters are the investigation of the dynamics in chemical reactions,[22,23] as well as probing solvent−solute interactions by photodissociation of molecules in/on rare-gas clusters.[24,25] Theoretical aspects concerning solvation—in particular nonadditive effects and open-shell dopants—are addressed by Bačić, Hutson, and co-workers,[26−30] prompted in part by recent experimental results of Nauta and Miller.[31]

We have measured the spectra of potassium-doped argon clusters, with the intent of adding to the series of potassium spectra already acquired in He droplets[32] and H_2/D_2 clusters.[33] As mentioned above, one can expect to observe a distribution of many different dopant species; many factors determine which spectra are observed, and with the present knowledge it is not always trivial to predict their outcome. Thus, these factors are interesting to study in their own right. In this manuscript we discuss explicitly the number of dopants per cluster, their location (surface vs inside), and spin state (high vs low).

In the course of this investigation we faced the need to separate and assign spectra that strongly overlap: for this purpose we devised the novel procedure reported here. We found that our spectra contain significant contributions from partially resolved bands that may be electronic transitions of K_3 never observed before, and we performed a set of *ab inito* calculations as a test.

Although there exists a considerable amount of published work on potassium-doped Ar matrices,[34−36] the only experimental work on alkali-atom-doped argon clusters are the LIF spectra of Na-doped clusters measured by Higgins:[37] he found only a weak monomer transition, dominated by two broadened (30−40 cm^{-1}) lines at the position of the gas-phase $3^2P_{3/2,1/2} \leftarrow 3^2S_{1/2}$ lines. More data exist for the alkaline-earth-metal atoms and molecules: electronic spectra of Ba on Ar clusters were taken by Visticot et al.,[38] of Ca and Ca_2 on Ar clusters by Gaveau et al.[39,40] Those authors find LIF spectra that are broadened and shifted from the free-atom/molecule case by a few hundreds of cm^{-1}, and they succeed in reproducing them with a model based on pair potentials,[6] combined with either classical molecular dynamics or Monte Carlo methods.

Theoretical work on alkali-doped rare-gas clusters exists in greater abundance; it should be noted, however, that most publications dealing with the simulation of absorption spectra of alkali-metal atoms and molecules in rare gas clusters address the case of dopants in highly symmetric environments *inside* the clusters,[41,42] and/or only in the presence of a small number of Ar atoms.[43] The latter authors treat also the case of Na on a close-packed [111] argon surface.

Spectra of singlet and triplet potassium dimers have been measured in helium nanodroplets;[12] some features in the spectra of potassium-doped matrices have been assigned to the singlet dimer.[44] Information on the geometric and electronic structures of matrix-isolated alkali-metal trimers was obtained from Raman,[45] and ESR[46−48] spectroscopy; the first record ever of K_3 are ESR spectra in an Ar matrix.[49]

Electronic spectra of gas-phase potassium trimers only exist (to our knowledge) as pump−probe photoionization measurements[50] probing the vibrational dynamics of doublet K_3. The
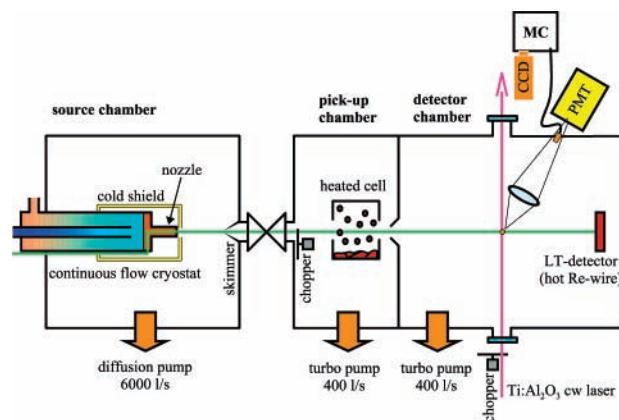

Figure 1. Schematic of experimental setup.

signal at zero delay between pump and probe (acquired at various photon wavenumber) can be taken as a coarse excitation spectrum. Otherwise, spectra have only been measured in He droplets and are limited to the quartet spin multiplicity.[51,52] No calculations exist of the level structure of K_3 in either spin multiplicity. It was suggested,[52] however, that the level structure of the lowest-lying states of Na_3 and K_3 should differ essentially by a scaling factor. A reasonable choice for this scaling factor is the ratio of the lowest atomic excitation energy. High-resolution[53−56] and extended[57,58] excitation spectra of gas-phase Na_3 have been measured, and the corresponding level structure calculated.[59] We test the applicability of such scaling by comparing our experimental spectra and *ab initio* calculations of the electronic structure of the K_3 doublet trimer with existing data on Na_3.

This manuscript is organized as follows: in section II we describe the experimental setup in detail. In section III we present the results of our work, further subdivided into (IIIA) experimental beam-depletion spectra, and their separation into monomer, dimer, trimer contributions; (IIIB) experimental LIF spectra; (IIIC) molecular dynamic simulations of the monomer absorption spectrum; (IIID) *ab initio* calculations of the electronic structure of K_3. In section IV we discuss our findings, separately for the monomer (where we further address the issue of spectral shifts and splittings), dimer (where we address the issue of spin multiplicity), and trimer. Section V contains a summary of our manuscript.

II. Experimental Section

The cluster beam apparatus we set up in Graz is primarily designed to investigate helium droplets. We want to give here a detailed description of it, irrespective of whether it is used to produce He droplets or Ar clusters; we will remark on the few existing differences when appropriate. The general principles of excitation and emission spectroscopy of alkali-metal atoms and molecules in He droplets have been described in detail in ref 12. A thorough analysis of the pickup cells' behavior turns out to be very important for spectral assignment.

The apparatus consists of two large vacuum chambers (Figure 1); the first is identified from now on as *source chamber*; the latter is further divided by an internal septum into two differentially pumped chambers, from now on referred to as the *pickup chamber* and *detector chamber*, respectively.

The source chamber is pumped by a baffled oil-diffusion pump (Leybold DI 6000/10 B, 6000 L/s nominal pumping speed) with water-cooled baffles (Varian 330, 3550 L/s nominal conductance), backed by a rotary/roots stack (Edwards EH1200/E2M80). The base pressure in the chamber is <10^{-6} mbar

without a beam and $\sim 10^{-3}$ mbar when a beam is present (all values as read by an ionization gauge, Granville Phillips GP274, controller GP307, uncorrected for ionization efficiency).

The pickup and detection chambers are separately pumped, each by a turbomolecular pump (Alcatel TMP5400, 400 L/s nominal; Leybold TMP361, 400 L/s nominal), backed by its own rotary pump (Alcatel 2012A and Leybold D16B, respectively). Base pressures in these chambers are, as measured, $< 10^{-7}$ mbar; they increase by less than an order of magnitude when a beam is present or when the alkali-metal ovens are in their stable operation condition.

Argon clusters with an average size $\bar{N} = 2 \times 10^3$ atoms (estimated through scaling laws[60]) are formed in a free-jet expansion of argon gas (AirLiquide, Alphagaz 2, grade 6.0) with a stagnation pressure of 60 bar through a 20 μm nozzle held at a temperature of 250 K. The nozzle is cooled by a continuous flow cryostat operating on liquid N_2; a gold plated shield cooled by the return vapor reduces radiative heat transfer. The nozzle is actively stabilized to the desired temperature (± 0.3 K) with a resistive heater; the temperature is measured at the nozzle tip with a silicon diode thermometer (Lakeshore DT-471, range 12) connected to a temperature controller (Lakeshore Model 330). For helium nanodroplets the average size range is $\bar{N} = 10^3 - 10^4$ He atoms, generated by expansion of helium gas (AirLiquide, Alphagaz 2, grade 6.0) with a stagnation pressure of 60 bar, through a 5 μm nozzle held at a temperature in the 14-20 K range. The cooling fluid is liquid helium.[96]

About 1 cm downstream of the nozzle, the beam passes through a 400 μm conical skimmer (Beam Dynamics, model 2) and enters the pickup chamber. There it is chopped for gated detection and doped. The pickup chamber contains two steel cells. Each is 4 cm long, is filled with about 1 g of the desired alkali metal, and can be independently heated by a resistor; its temperature is monitored by a cladded thermocouple (Type K, Omega Engineering, Inc.) and actively stabilized by a temperature controller (Omega, Models CN77323 and CN76020, respectively). The cell mounts are designed to minimize heat leakage to the chamber, as well as cross-talk between cells; we observe that, under vacuum, the temperature of the unheated cell will increase by less than 5 °C when the other is heated from room temperature to operational temperature. We used quartz cells in earlier experiments, with no notable difference.

The cell containing K metal is operated between 140 and 240 °C, where the tabulated equilibrium vapor pressure of pure K is between 10^{-1} and 10^{1} Pa ($10^{-3} - 10^{-1}$ mbar).[61] In principle, the vapor pressure and density inside the pickup cell can be determined via the temperature of the cell, assuming thermodynamic equilibrium. In our case this appears to be a poor approximation, probably because of large entrance and exit holes (5 mm diameter), a large surface/volume ratio of the molten metal inside the cell, and the fact that part of the metal may be covered with a layer of oxide. We observed that the pressure in the pickup cell must be kept higher by a factor of ≈ 15 for Ar clusters, as compared to He. We estimate that the different average cluster size in the two experiments is sufficient to account for this factor. MD simulations (see below) do not seem to indicate a sticking coefficient significantly smaller than 1 for collisions between K atoms and Ar clusters. Another observation we made is that alkali-metal consumption caused the vapor density in the pickup cell to decrease, despite constant oven temperature, by 10-20% per experiment, as monitored by a surface ionization detector (see below).

Doped clusters enter the detection chamber through a second skimmer (5 mm diameter, homemade) such that differential

pumping is maintained. Doped clusters are excited by crossing the supersonic beam at right angle with the well collimated beam (1-3 mm^2 cross section) from a cw Ti:Al$_2$O$_3$ ring laser [Coherent 899-01, with short-wave (11900-14200 cm^{-1}) and midwave (10500-12500 cm^{-1}) mirror sets], pumped by an Ar$^+$ laser (Coherent Innova 200) power-stabilized at 15 W multiline visible. The Ti:Al$_2$O$_3$ laser is operated in broadband mode (nominal line width: 8-12 GHz), with the birefringent filter as the sole tuning element. The wavenumber is scanned by rotating the birefringent filter with an electrical motor attached to a reducing gearbox, at typical scanning speeds of 0.2-4 cm^{-1} s^{-1}. The absolute wavenumber $\tilde{\nu}$ is measured with a commercial wavemeter (Burleigh WA 1500, specified limit accuracy $\pm 1 \times 10^{-7}$); the readings fluctuate within the nominal line width of the laser. The typical output power, which is not actively stabilized, depends on the mirror set as well as on the tuning curve of the crystal and varies between 200 mW and 3 W. The relative laser power across a scan is measured with a photodiode calibrated against a commercial power meter (Coherent LabmasterE, LM-2-VIS head) and is used to normalize the spectra, which we verified not to be saturated.
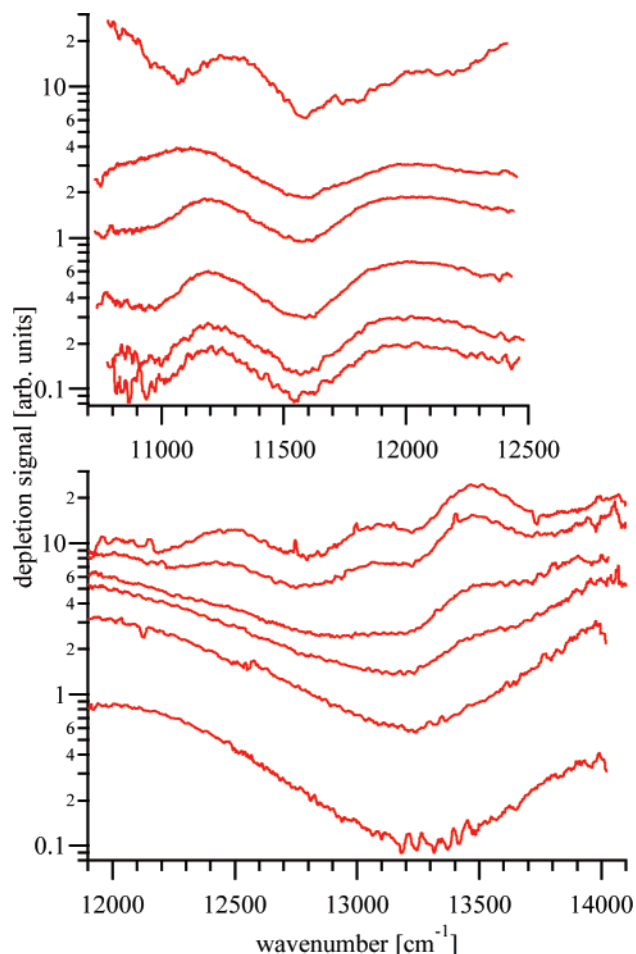
Windows at Brewster angle, baffled entrance, and exit tubes, along with spatial filtering in the collection system, minimize the scattered light reaching the detector [typical: 10^4 (counts/s)/W at 1.4 kV photomultiplier voltage], whose effect is further reduced by mechanically chopping the droplet beam and performing a differential measurement of the photon count. Laser-induced fluorescence is collected by a lens system with 10% collection efficiency and suitably re-imaged to fill the active area of a Peltier-cooled photomultiplier (housing, Products for Research, TE210TS-RF; tube, Hamamatsu R943-01 with GaAs photocathode). Single-photon pulses go through a fast pre-amplifier (Ortec, 9301) and amplifier/discriminator (Ortec 9302) and are then counted by a homemade 15-bit counter, operated in 2-channel mode. The droplet beam is chopped at 22.7 Hz, and the counters are gated for exactly 20 ms. This gating time is intentionally shorter than the chopper half period, so as to eliminate counts at the modulation edges. Data acquisition is controlled by a personal computer running LabVIEW.

For emission spectra, the photomultiplier is replaced by an optical fiber bundle funneling the light into a 0.35 m spectrograph (McPherson EU/700) equipped with a liquid-nitrogen-cooled CCD detector (Princeton Instruments, LN/CCD-1100PR/VIS/IR/PB-1). Although in principle the detector is suitable for hour-long acquisition, and long integration is desirable to minimize readout noise, in practice signal contamination from cosmic rays is a major limiting factor. Spectra of 30 s each (resulting in 1 or 2 cosmic ray events per spectrum) are acquired in binning mode; pixels containing a cosmic ray event are discarded, and then as many spectra as necessary (10-50) are averaged together to achieve the desired signal-to-noise ratio.

A surface ionization, or Langmuir-Taylor (LT), detector is located further downstream to detect the depletion of the doped beam signal upon excitation. It consists of a resistively heated (current mode, 1.4 A typical) rhenium ribbon (anode) surrounded by a collector shield (cathode) made of solid copper, with entrance and exit holes for the cluster beam. Alkali-metal atoms impinging on the hot ribbon are ionized with probability close to one[62] and accelerated toward the collector (the bias voltage between anode and cathode is established with a commercial 9 V battery), where their recombination current I_{LT} is detected with a picoammeter (Keithley 414S, response time < 0.14 s).

Assuming, as is reasonable, that excitation of alkali-metal atoms/molecules on the surface of a rare gas cluster always
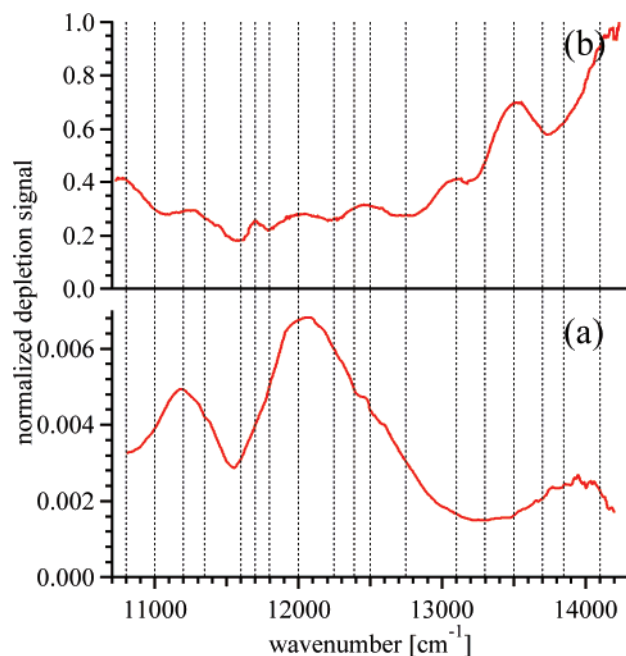
Figure 2. Beam-depletion spectra of K atoms and molecules on argon clusters at increasing vapor pressure in the pickup cell. Upper panel: Scan with laser midwave optics. Lower panel: short-wave optics. Note the logarithmic vertical scale. Cluster source conditions: 240 K, 60 bar.

Figure 3. Beam-depletion spectra of K atoms and molecules on argon clusters over the entire laser range. Upper panel: high pickup pressure (I_{LT} = 65 nA). Lower panel: low pickup pressure (I_{LT} = 0.2 nA). Vertical bars indicate wavenumbers at which signal growth is analyzed. Cluster source conditions: 240 K, 60 bar.

results in their photodetachment, a depletion of the overall beam signal will be detected; the resulting beam-depletion (BD) spectrum can be considered a faithful representation of the overall absorption spectrum. Phase-sensitive detection is necessary: it is done by chopping the laser beam and using a lock-in amplifier (Ithaco Dynatrac 391A or Stanford SRS510). The large time constant of the picoammeter makes it necessary to operate the laser chopper wheel at low frequencies (about 10 Hz), which results in less-than-optimal noise suppression. Detector performance is limited by the output noise of the picoammeter at low oven temperatures and by the large dc component of the ion current (from the high alkali-metal background in the detector chamber) at high oven temperatures.

III. Results

A. BD Spectroscopy. The search of an unknown spectrum always proceeds from reasonable guesses based on known systems similar to the one being investigated. We initially relied on the beam-depletion spectra of K atoms in D_2 clusters.[33] There, two main peaks were observed: the first $\approx$200 cm^{-1} wide and $\lesssim$100 cm^{-1} red-shifted from the gas-phase position of the 4S– 4P multiplet; the second twice as broad and blue-shifted by $\approx$400 cm^{-1}. No spin–orbit splitting (57.706 cm^{-1}, ref 63) was resolved. As the host-dopant interaction is of the van der Waals type, we expected the shift values to scale roughly with the

electric-dipole polarizability of the host atom/molecule (Ar, 1.64 Å^3; D_2, 0.79 Å^3; ref 61), i.e., to be approximately a factor of 2 larger for Ar clusters (also compare the well depths of the K–H$_2$ and K–Ar pair potentials: 16 and 40 cm^{-1}, respectively[64,65]).

BD spectra were measured at a set of different pickup conditions. The full wavenumber range was covered with two sets of laser optics; note that because substitution of a set is quite a time-consuming operation, the series shown in the two panels of Figure 2 have been taken in different experimental runs. For the sake of presentation clarity, the raw data have been smoothed considerably, on the basis that no finer structure is observed in the spectra.

We also acquired a few continuous spectra with the slower approach: the two portions of each full spectrum were sequentially measured, at fixed pickup conditions, then spliced by scaling the traces to overlap in the common scanning range 11900–12400 cm^{-1} (Figure 3).

One immediately notices the overwhelming breadth of individual peaks, as well as the complex evolution of the whole spectrum with increasing pickup pressure. We will now discuss the separation of the spectrum into its atomic and molecular components. As the cell temperature T_c was found not to be a stable indication of pickup conditions, we chose to take the surface-ionization-detector current I_{LT} to describe the conditions in the cell, an approach which we will work out in more detail during this section.

Panel a of Figure 3 shows the BD spectrum taken at I_{LT} = 0.2 nA, which will be referred to as the *low-density spectrum* (LDS). This value of I_{LT} corresponds to the lowest alkali-metal atom vapor pressure at which a spectrum could be measured with sufficient signal-to-noise ratio. One can observe three broad ($\gtrsim$500 cm^{-1}) peaks at 11250, 11950, and 13950 cm^{-1}. Panel b shows the BD spectrum at I_{LT} = 65 nA, which will be referred to as the *high-density spectrum* (HDS). The absorption signal has grown by about 2 orders of magnitude, and its shape has changed completely. The HDS shows several overlapping peaks

at about 11700, 12500, 13000, 13500, and 14100 cm^{-1}, and another one can be inferred at the red end of the scanning range of the laser.

The decomposition and assignment of spectral features is considerably more complicated than in studies of He clusters, where one has sharp intense spectra, which seldom overlap. There, it is easier to assign the spectra even in the presence of several different species. As the perturbation induced by the helium is smaller, assignment can be achieved by combining the pressure dependence of signals, and the associated change of capture probability for a given number of atoms, with some knowledge of related gas-phase spectra.

As discussed in ref 10, the contribution of *n*-mers to the overall signal intensity at wavenumber $\tilde{\nu}$, which we will call $S_n(\tilde{\nu})$, depends on the partial pressure p in the pickup cell (a convenient, if slightly inaccurate, substitute for the density ρ) in a manner determined by the probability for successive capture of n atoms:

$$S_n(\tilde{\nu},p) \propto \frac{(p/p_1)^n}{n!} \exp(-p/p_1) \tag{1}$$

p_1 being the pressure at which the probability of a single pickup is the largest.

Usually the cell temperature T_c is used to calculate p via a known parametrized function:

$$\log(p/\text{atm}) = A_p + B_p/T_c \tag{2}$$

with $A_p = 4.402$ and $B_p = -4453$ K for potassium.[61] Equation 2 describes the equilibrium vapor pressure of the substance, and deviations can be expected for a cell opened into a vacuum. As mentioned, we observed that on different days different T_c were necessary to obtain comparable pickup conditions. Besides, T_c is an inconvenient control parameter in that the variable to be controlled, the pickup probability, is a strongly nonlinear function of it and also exhibits a considerable time lag. I_{LT} is a desirable control parameter: first, it is fast reacting; second, one expects it to be approximately linear with the pickup probability, and to give good reproducibility. Ideally, p and I_{LT} should be both good estimators of the pickup probability, that is, they should only differ by a scaling factor. Upon a slow and careful scan of the cell temperature, we found that log I_{LT} has the same inverse linear dependence on T_c as p:
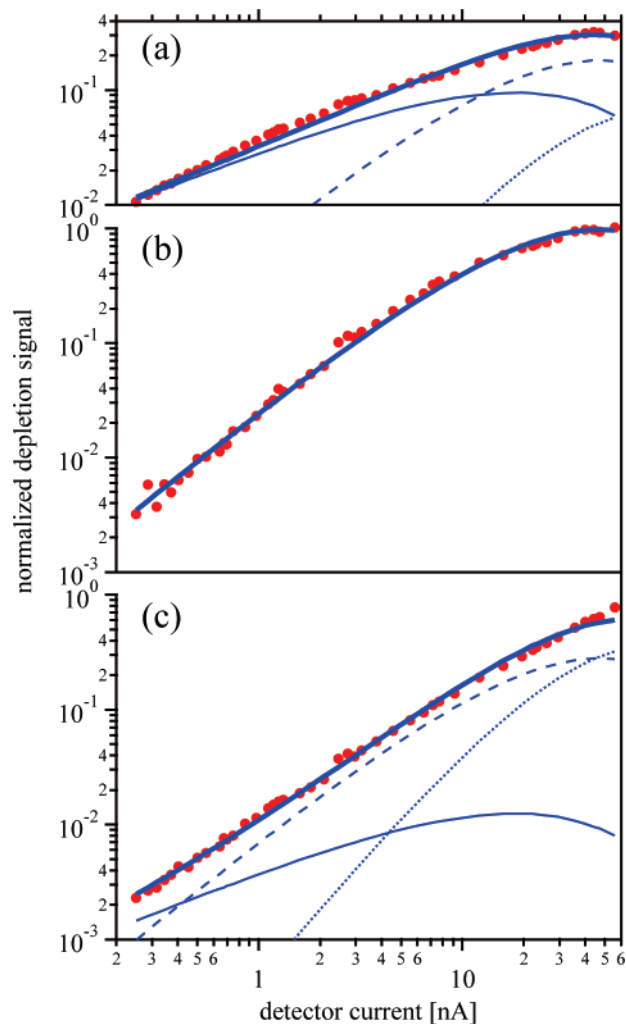
$$\log(I_{LT}/\text{nA}) = A_I + B_I/T_c \tag{3}$$

with $B_I = -6104$ K; $A_I \sim 15$ varies between experimental runs. The most general dependence between p and I_{LT} that can be derived from eqs 2 and 3 is a power law:

$$p/p_1 = (I_{LT}/I_1)^k \tag{4}$$

with $k = B_p/B_I = 0.73$, and I_1 the current at which the probability of a single pickup is the largest (also varies between different runs).
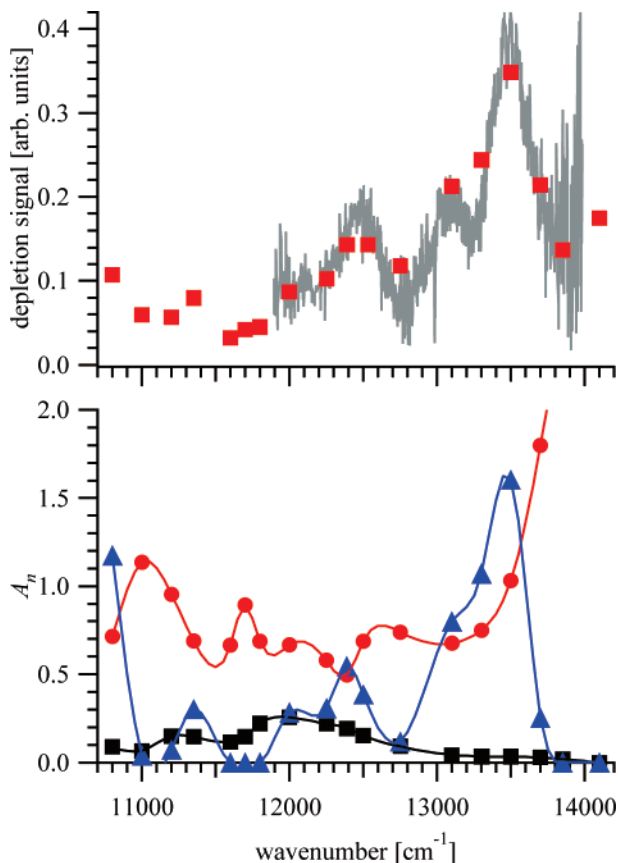
We tested this power-law dependency on the well-resolved spectra of Rb on He droplets and found that, in the temperature range 140−220 °C, eq 4 with $k = 0.717$ gives a good description of the pickup probability. This value is also close to the value, 0.725, we extract from the spectral separation procedure described below. We note that the formula for the flux out of an effusive source[66] would predict $I_{LT} \propto pT_c^{-1/2}$, that is $k = 1$ if we neglect the $T_c^{-1/2}$ dependence, on account of the small temperature range.

Figure 4. Decomposition of spectral contributions at (a) 12000, (b) 14100, and (c) 13500 cm^{-1}: circles, experimental data; thick line, best fit (eq 5); thin solid line, monomer fraction; dashed line, dimer fraction; dotted line, trimer fraction. In (b) the monomer and trimer fractions are strictly zero, and the best fit curve coincides with the dimer fraction. The best-fit value of common parameters is $k = 0.725$, $I_1 = 18.08$ nA.

To process and separate the spectra using a model based on eqs 1 and 4, it was necessary to get data points at as many different pickup pressures as possible. We reckoned that for the analysis to be meaningful, all the data had to be acquired in one run. The normal procedure, that is, to set a cell temperature, to wait until the system has equilibrated, and then to acquire a full spectrum, would imply a prohibitively long time. We thus chose to cyclically sample $S(\tilde{\nu},I_{LT})$ at 11 representative wavenumbers (indicated in Figure 2 by vertical bars, and corresponding to peaks and valleys in the LDS and HDS) while the cell was being heated and I_{LT} was slowly increasing from 0.25 to 56 nA. The sampling time was 45−60 s per data point. For practical reasons this first series was taken using the short-wave optics set. After equilibrium was reached at $I_{LT} = 65$ nA, we switched to the midwave optics set, then let T_c decrease, and sampled 8 further wavenumbers.

To rule out hysteresis effects between heating and cooling, we compared $S(\tilde{\nu},I_{LT})$ at 12000 cm^{-1}, where both mirror sets work. The two series overlap nicely, showing that I_{LT} provides a good estimator of the pickup probability even for dynamic pickup conditions. A systematic error intrinsic to this method is the variation of pickup pressure during one measurement cycle. This is setting a limit to the sampling time per data point, as well as to the number of sampled wavenumbers.

Optical Spectroscopy of Potassium-Doped Ar Clusters

J. Phys. Chem. A, Vol. 111, No. 49, 2007 **12391**

Figure 5. Results of decomposition procedure (eq 5). Lower panel: $A_n(\tilde{\nu}_i)$ factors representing spectral contributions from potassium monomers (squares), dimers (circles), and trimers (triangles). The lines are spline interpolations, meant as guides to the eye. Upper panel: Comparison of an experimental BD spectrum (gray trace) with a simulated one (red squares) at $I_{LT} = 250$ nA. This spectrum was measured with the midwave optics set only.

A least-squares fit was applied simultaneously to all $S(\tilde{\nu}_i, I_{LT})$ growth curves ($i = 1.19$), with a function derived from eqs 1 and 4:
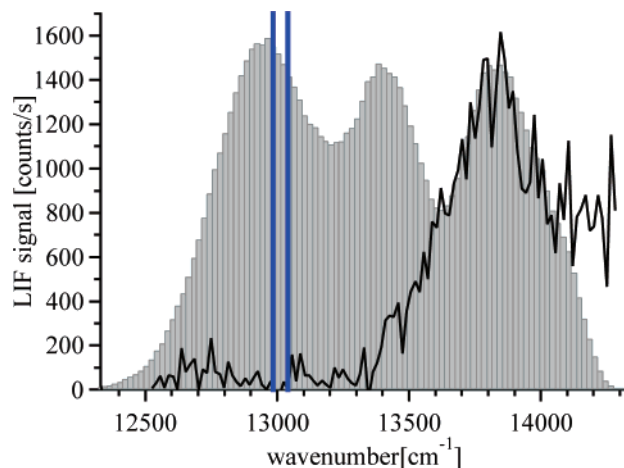
$$S(\tilde{\nu}_i, I_{LT}) = \sum_{n=1}^{3} A_n(\tilde{\nu}_i)\frac{x^n}{n!}\exp(-x) \quad (5)$$

$$x = (I_{LT}/I_1)^k \quad (6)$$

with the amplitudes $A_n(\tilde{\nu}_i)$, I_1, and k as free parameters. I_1 is a common parameter shared by all growth curves; we recall that its best fit value (18.08 nA) should be interpreted as the value of I_{LT} for which the pickup probability of one dopant per cluster is the largest, and that the best fit value of k is 0.725. The factors $A_n(\tilde{\nu}_i)$ represent the intensity of the n-mer spectrum at wavenumber $\tilde{\nu}_i$.

Figure 4 shows the results of the decomposition procedure for three selected wavenumbers: in panel a the slowest relative increase in beam-depletion signal is observed, indicating a major monomer contribution ($\tilde{\nu} = 12000$ cm^{-1}). The decomposition is, however, able to reveal that non-negligible contributions from larger oligomers are also present, which emphasizes once more the strong overlap of all spectra. Panels b and c display growth curves with pure dimer contribution ($\tilde{\nu} = 14100$ cm^{-1}) and significant trimer contribution ($\tilde{\nu} = 13500$ cm^{-1}), respectively.

Figure 5 shows the best-fit values of $A_n(\tilde{\nu}_i)$ with $n = \{1, 2, 3\}$, which we identify as the spectra of K, K_2, and K_3. To test

Figure 6. Black line: LIF excitation spectrum of potassium-doped argon clusters measured at $I_{LT} = 3$ nA. Vertical bars near 13000 cm^{-1} mark the positions of the gas-phase atomic D lines. Histogram, arbitrary scaling: MD simulation of the absorption spectrum of a K atom on a cluster of 190 Ar atoms.

the predicting abilities of the model described by eq 5, we calculated $S(\tilde{\nu}_i, I_{LT})$ at $I_{LT} = 250$ nA, a value 4 times higher than the largest included in the fit. We compare this simulation with an experimental spectrum taken in an early run at corresponding pickup conditions (upper panel). The good agreement between model and experiment convincingly demonstrates the applicability of growth analysis in a wide range of pickup conditions, which makes assignment of spectral contributions unambiguous.

B. LIF. In the entire investigated spectral range (10700−14100 cm^{-1}) the only feature showing fluorescence above the sensitivity limit of the PMT was a band starting from 13300 cm^{-1} and extending to the blue beyond 14300 cm^{-1} (Figure 6). Dispersed fluorescence revealed that within the sensitivity of detection the emission originates from free K atoms only. The presence of further emission, broadened below the sensitivity limits, cannot be excluded. We note that the gas flow (atoms/s) corresponding to our source conditions is approximately the same as in He experiments; however, the integrated LIF spectrum here is about 50 times weaker.

No growth analysis could be performed for the LIF spectrum, and it is noteworthy that its shape has no resemblance with any of the spectral features observed in BDS or predicted by decomposition analysis. We are not in the position to further characterize this spectrum experimentally; therefore its assignment can only be tentative. A few arguments in favor of the monomer will be made by comparison with MD simulations.

C. Modeling of K on Ar$_N$. To estimate qualitatively the electronic excitation spectrum of the monomer, we carry out a simple classical MD simulation combined with pairwise-additive potentials, similar to the approach described in ref 38. Numerical integration of the equations of motion is done with a homemade code implementing the leapfrog algorithm (eqs 7 and 8) where explicit calculation of velocities allows coupling to a thermal bath:[67,68]

$$\vec{v}_i\left(t + \frac{\Delta t}{2}\right) = \vec{v}_i\left(t - \frac{\Delta t}{2}\right) + \Delta t\frac{\vec{F}_i(t)}{m_i} + \mathcal{O}(\Delta t^3) \quad (7)$$

$$\vec{r}_i(t + \Delta t) = \vec{r}_i(t) + \Delta t\vec{v}_i\left(t + \frac{\Delta t}{2}\right) + \mathcal{O}(\Delta t^4) \quad (8)$$

The position $\vec{r}_i$ and velocity $\vec{v}_i$ of the ith atom, of mass m_i, under the action of the force $\vec{F}_i$ are computed every $\Delta t = 3$ fs. $\vec{F}_i$ is

12392 *J. Phys. Chem. A, Vol. 111, No. 49, 2007*

Nagl et al.

TABLE 1: Lennard-Jones Parameters for the Ar−Ar Potential and Morse Parameters for the M−Ar Pair Potentials (D_e, ω_e in cm^{-1}; R_e in Å)^a

	XΣ			BΣ			AΠ		
	D_e	R_e	ω_e	D_e	R_e	ω_e	D_e	R_e	ω_e
Ar^b	97.8	3.75	−						
K^c	59	5.13	10.28	34	7.26	7.32	440	3.41	56.93
Ca^d	87.0	4.86	18.31	36.1	5.69	10.11	87.8	4.62	14.70
Ba^e	73	5.55	16	12	10.6	3	90	5.40	16

^{a} The XΣ values for K−Ar are for comparison only, as the potential of ref 65 is used instead in the molecular dynamics simulation. ^{b} Reference 69. ^{c} Reference 70. ^{d} Reference 71. ^{e} Refrerence 72.

computed as the sum over all atoms of the derivative of the appropriate two-body interaction potential: a 6-12 Lennard-Jones potential for Ar−Ar (from ref 69); the HFD potential as given in ref 65 for K−Ar ground state. Morse potentials, without spin−orbit coupling, are chosen for excited states (from ref 69); the related parameters are reported in Table 1. The ground-state minimum of K−Ar occurs at an atomic distance where the excited B^{2}Σ state is strongly repulsive, thus poorly reproduced by the Morse potential: for the B^{2}Σ potential only, at distances <11 Å, we choose to use an interpolation of experimental data^{73} instead of the Morse formula.

Clusters containing $N = 190$ argon atoms are used in the calculation. To achieve an average cluster temperature $\bar{T}$ of 35 K, velocity scaling^{68} is applied at each time step until $T = \bar{T}$:

$$\vec{v}_i(t+\Delta t/2) \rightarrow \gamma \vec{v}_i(t+\Delta t/2) \quad (9)$$

with the scaling factor

$$\gamma = (\bar{T}/T)^{1/2} \quad (10)$$

where the actual temperature T is calculated from the kinetic energy of the N argon atoms in a cluster:

$$T = \frac{2}{k_B(3N-6)} \sum_{i=1}^{N} \frac{m_i v_i^2}{2} \quad (11)$$

Simulation of the collision process of these clusters with a K atom (head-on collision, at a relative velocity of 1000 m/s) showed a capture probability of 100%; further, the atom did not penetrate the cluster, in agreement with the findings of ref 18. After collision, the system is allowed to evolve for 5000 time steps (15 ps) to ensure complete thermalization of the K atom. At each subsequent step, until a total time of 0.3 ns has elapsed, the instantaneous excitation energies of the K atom are computed and binned in a histogram.

The ground-state energy of the K atom is simply given by summing the K−Ar ground-state pair potential over all Ar atoms. A similar sum over excited-state pair potentials, with the perturbation approach presented in ref 43, yields a 3 × 3 Hamiltonian; its diagonalization at each time step gives the instantaneous energies of the three excited states. To rule out metastable behavior, a set of 26 clusters has been prepared. Figure 6 shows the histogram of the calculated excitation energies, which is the representation of the absorption spectrum. The result shows, as expected, a triplet peak structure, with the center-of-gravity of the band shifted to the blue of the atomic gas-phase lines by 330 cm^{-1}.

D. CASSCF Calculations. Extensive electronic structure calculations on (pure and mixed) trimers and tetramers of Li and Na, and on several lithium hydrides, were performed by

Gaus.^{74} His work contained several 2-dimensional scans of the ground electronic state of Na$_3$ near the equilibrium position, notably vs the normal coordinates Q_x and Q_y (symmetric bending and asymmetric stretch), as well as scans vs Q_x of excited states, at the CASSCF level (complete active space self-consistent field).
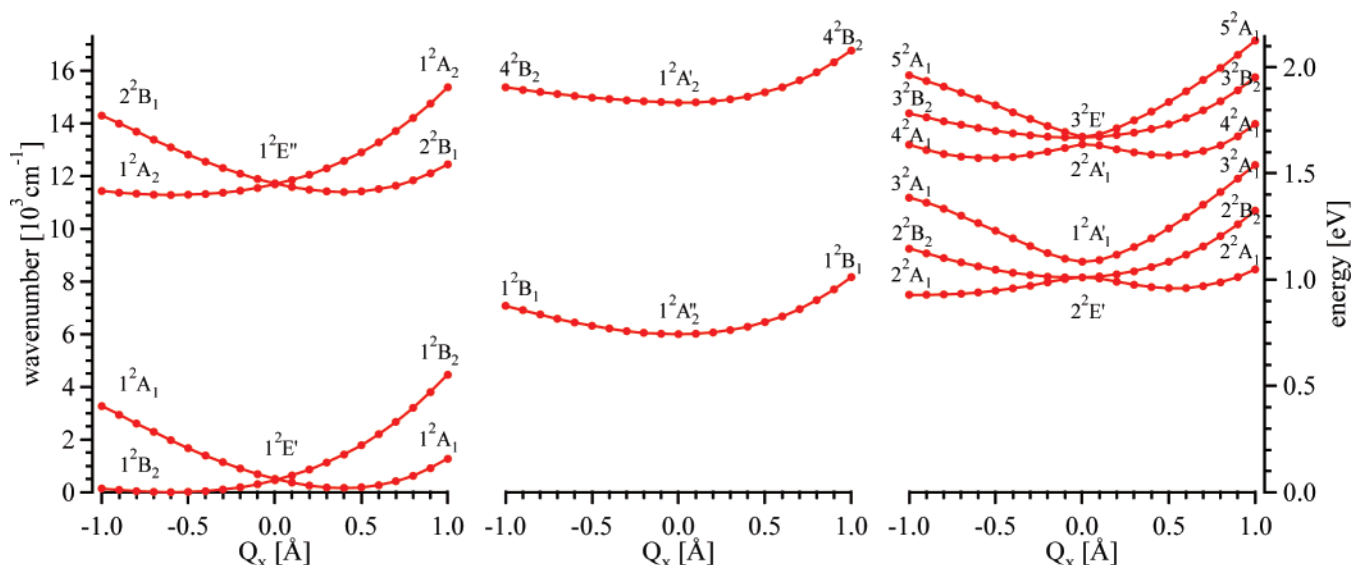
Scans of the ground-state electronic surface of K$_3$ using a density functional approach were performed by Martins et al.^{75} Equilibrium structures of small ($n \leq 6$) alkali-metal clusters were investigated by Spiegelmann and Pavolini at the CASSCF level.^{76}

We performed two-dimensional scans, over (Q_s, Q_x) (breathing mode and symmetric bending mode) and (Q_x, Q_y), of the ground-state electronic surface of K$_3$ at the UCCSD(T) level of theory (unrestricted coupled cluster calculations with single, double and non-iterative triple excitation), as well as scans of the first 12 electronic states over Q_x near the equilibrium position, applying the CASSCF method of Werner and Knowles$^{77-80}$ as implemented in the MOLPRO^{81} package. The details of the calculation will be published separately. In short, we used the relativistic small-core ECP (effective core potential) basis set ECP10MDF of the Stuttgart/Cologne group^{82} augmented with three additional diffuse functions (s,p,d), using the even-tempered scheme implemented in MOLPRO. The even-tempered exponent for these additional functions is based on the ratio of the two smallest exponents in the original set. Using the basis set in its fully uncontracted form leads to the scheme (12s,12p,6d,3f).

We gauge the accuracy of the basis set by a series of test calculations on atomic K, and on K$_2$ dimers. At the UCCSD-(T) level, we reproduce the atomic polarizability $\alpha = 290.7$ (experimental^{83} $\alpha = 290.2 \pm 8$), the singlet-K$_2$ equilibrium bond length $r_e = 3.93$ Å, and binding energy $D_e = 4299$ cm^{-1} (experimental^{84} $r_e = 3.93$ Å and $D_e = 4450$ cm^{-1}). The dimers' results are corrected with respect to the BSSE (basis set superposition error) using the counterpoise correction of Boys and Bernardi.^{85} At the CASSCF level, including second-order perturbation corrections (CASPT2, ref 86), we reproduce the 4s−4p, 4s−5s, and 4s−3d electronic excitations of the atom within respectively +5, −73, and +76 cm^{-1} of the spin−orbit averaged experimental values.^{63}

The ground-state UCCSD(T) scan with further geometry optimization finds the absolute minimum for K$_3$ at an obtuse isosceles geometry (C_{2v}, ^{2}B$_2$ symmetry), with bond length $b = 4.322$ Å and bond angle $\theta = 74.0°$ (corresponding to $Q_s = 4.59$ Å, $Q_x = -0.61$ Å, $Q_y = 0$). For comparison, the density functional calculations of Martins et al.^{75} find $b = 4.0$ Å and $\theta = 77°$. At fixed C_{2v} symmetry, we find a relative minimum 165 cm^{-1} above the absolute minimum, at bond length $b = 4.783$ Å and bond angle $\theta = 51.8°$, which turns out to be a saddle point on the three-dimensional energy surface. Martins et al. find $b = 5.4$ Å, $\theta = 41°$, and an energy difference between absolute minimum and saddle point of 160 cm^{-1}.

A [3,23]-CASSCF scan over the Q_x coordinate with Q_s fixed to its global minimum value of 4.59 Å shows a level structure very similar to that calculated by Gaus,^{74} and by Cocchini et al.,^{59} for Na$_3$. We estimate the error due to a finite active space through the observation that the trimer's electronic states correlating to the 4P atomic asymptote (scan over the Q_s coordinate up to $Q_s = 30$ Å, at Q_x, $Q_y = 0$) converge to a value of 11550 cm^{-1}, that is 1493 cm^{-1} lower than the spin−orbit averaged experimental value.^{63} We force consistency with the experimental asymptotic value by adding the above difference to all the states, except 1 ^{2}B$_2$ and 1^{2}A$_1$. In Figure 7 we present

Figure 7. Calculated potential energy curves of K_3, scanned along the Q_x normal coordinate at $Q_s = 4.59$ Å and $Q_y = 0$: left: two-state distortion; center: nondegenerate states; right: three-state distortion. The curves are labeled according to their C_{2v} symmetry (D_{3h} at $Q_x = 0$) and grouped according to their Jahn−Teller distortion pattern.

the resulting calculated curves, grouped, as in the work of Cocchini et al.,[59] according to their Jahn−Teller distortion pattern. We will compare our CASSCF calculations with our experimental data, and with existing Na_3 data (appropriately scaled) in section IVC.

IV. Discussion

A. Monomer Spectrum. Not surprisingly, the spectrum we assign to the potassium monomer closely resembles the LDS, of which it should be the limiting case for zero pickup pressure. The largest difference is observed at the blue end of the spectral range, where the contribution from the dimer is significant. The spectrum consists of two partially resolved peaks at ≈ 11250 and ≈ 12000 cm^{-1}, the latter with a broad shoulder to the blue. The spectrum is strongly shifted from, and nearly at a minimum around, the atomic gas-phase lines. This observation is unexpected and differs greatly from the spectra of K on H_2 and D_2 clusters, as well as from those of alkaline-earth-metal atoms on Ar clusters. We will comment on the shift at the end of this section and first discuss the structure of the spectrum.
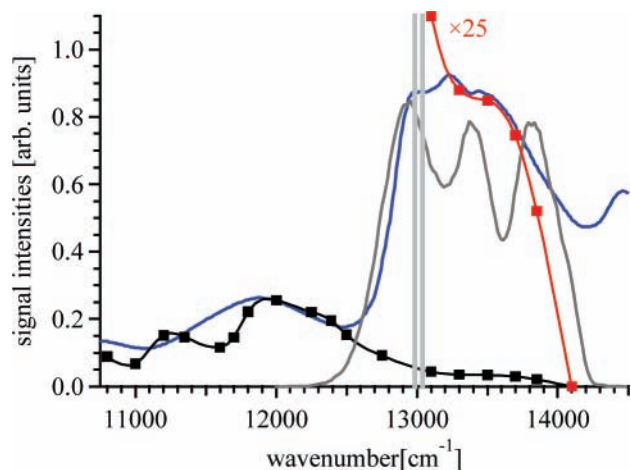
Doublet and triplet peak structures in the vicinity of the free atomic transitions are common for atomic spectra of alkali-metal-doped matrices, and reflect a splitting of the triply degenerate $nS-nP$ transition.[44] In a matrix, trapping sites are usually highly symmetric, and the multiplet should remain degenerate; peak splittings are nevertheless observed. A critical evaluation of the mechanisms that can explain the splitting has been given by Boatz and Fajardo.[43] Because of the tight trapping structure, splittings tend to be large, and the center of gravity of the multiplet is shifted, usually to the blue, by a smaller amount. For K in Ar, two triplets have been observed and named "red" and "blue" triplet, respectively, after their relative position in the visible spectral range.[36] Only the former falls within the scanning range of our laser; the latter will not be further considered for comparison with our spectra. We note that comparison of our results with those involving K in an Ar matrix should be done with prudence: argon matrices become unstable at temperatures as high as those of argon clusters,[44] and dopant atoms tend to migrate and aggregate; thus atomic absorption data are, to our knowledge, only available for lower tempera-

tures. More important: in our case K resides on the cluster surface rather than inside.[18]

A surface location of alkali-metal atoms is the *de facto* standard in the case of atoms on He or molecular-hydrogen clusters. Here a simple but effective description of the electronic absorption spectrum has been devised: that of a pseudodiatomic molecule, with the whole cluster playing the role of one of the atoms. The system has cylindrical symmetry and the triple degeneracy of the excited state of the alkali-metal atom is only partially lifted, if spin−orbit coupling is neglected. The peak observed closer to the gas-phase lines, slightly red-shifted in the case of H_2, corresponds then to bound−bound transitions, the blue-shifted peak to bound-free transitions.[32] The internal degrees of freedom of the cluster are obviously neglected, except to empirically account for the smearing of otherwise discrete transitions. A similar approach, based on MD calculations, was tried for alkaline-earth-metal atoms on Ar_N[38,39] to successfully model the observed LIF; it was found that these atoms remain on the cluster surface and that the spectrum splits into a line triplet, with shifts, splittings, and widths of a few hundred cm^{-1}. Notwithstanding the different electronic configuration, these atoms are closely related to K, as far as their interaction with Ar is concerned (we report in Table 1 the relevant Morse-potential parameters), and we will use those results to help interpret our spectra.

With the same approach as that of refs 38 and 39 we find, as expected, a triplet splitting of the otherwise degenerate transition, with the center of the band blue-shifted by about 330 cm^{-1} and each of the three peaks having a width of 330 cm^{-1} (Figures 6 and 8). The modeled spectrum resembles the "red" triplet seen in matrix absorption (Figure 8), and our LIF spectrum overlaps with just the highest-wavenumber peak of such a triplet (Figure 6). This is reminiscent of the spectra of Na and K on molecular hydrogen clusters, where only free-atom fluorescence from the bluemost portion of the excitation spectrum was observed.[33] It was then argued that most fluorescence would be quenched or red-shifted out of the spectral window of the detector. If indeed our LIF spectrum originates from the K monomer, then the onset of fluorescence can be used to roughly estimate the binding energy of the K atom to the cluster, with the same argument

Figure 8. Comparison of monomer spectral component (black squares and spline interpolation, same as Figure 5; red squares and line, ×25 magnified), with the absorption spectrum of a potassium-doped argon matrix (blue thick line, from ref 36) and with MD calculations (gray line). The vertical bars near 13000 cm^{-1} mark the positions of the gas-phase lines. The relative scaling of signals is arbitrary.
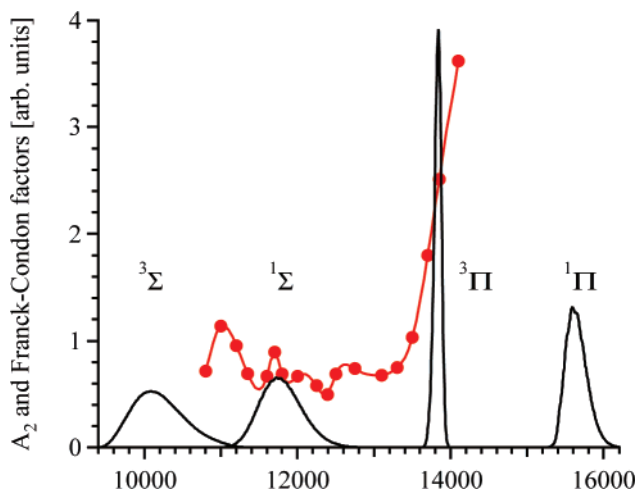

Figure 9. Comparison of dimer spectral component (circles and spline interpolation, same as Figure 5) to calculated excitation spectra of K$_2$ molecules in gas phase (at 35 K, details in text).

made for Na atoms desorbing from He nanodroplets.[87] Fluorescence begins 360 ± 60 cm^{-1} above the center of gravity of the gas-phase D lines: the value is consistent with the binding energy estimated from our MD simulations (340 cm^{-1}).

Altogether, we can only compare our experiments and simulations to existing ones that differ from ours in at least one major condition: either a different cluster constituent (He, H$_2$/D$_2$) or a different dopant atom (Na, Ba, Ca) or a different location (bulk vs surface). Despite these limits, from all of the above we would expect that the 4P−4S transition of a K atom on an Ar cluster be located energetically close to the free-atom lines. Indeed, the weak blue shoulder of the BD spectrum does overlap with both the matrix "red triplet" and our MD simulation; we consider it thus a reasonable candidate for the monomer spectrum.

Based on the growth analysis, the rest of the spectrum, which accounts for most of the overall intensity, must also contain only one K atom, but the extent of red shift is hard to rationalize as due to the Ar cluster alone. One needs a significant charge transfer, that is, impurities such as H$_2$O. We verified with basic single-point CASSCF calculations that the 4S−4P transition of a free K−H$_2$O complex is indeed red-shifted by ∼2000 cm^{-1}. Although the presence of water in the experimental chamber could be easily justified, it is difficult to explain why its contributions to the spectrum should be dominant. This portion of the spectrum overlaps with a part of the matrix spectrum that was assigned to singlet K$_2$ (ref 36); we believe either this overlap to be accidental or the assignment of ref 36 (where this feature disappears upon annealing) to be incorrect.

In summary, with our present knowledge, we tentatively assign the "monomer component" to a K atom on the surface of an argon cluster, allowing the possibility that part of it is due to a complex with a strongly interacting impurity such as a water molecule.

B. K$_2$. The spectral contribution we assign to the potassium dimer is rather unstructured—except for a prominent rise at the blue end of the scanning range, so it is not possible to make further statements for its assignment. We only note that for the free dimer there are two triplet−triplet and one singlet−singlet transition within our scanning region; a further singlet−singlet transition may have to be considered if large red shifts are allowed (Figure 9).
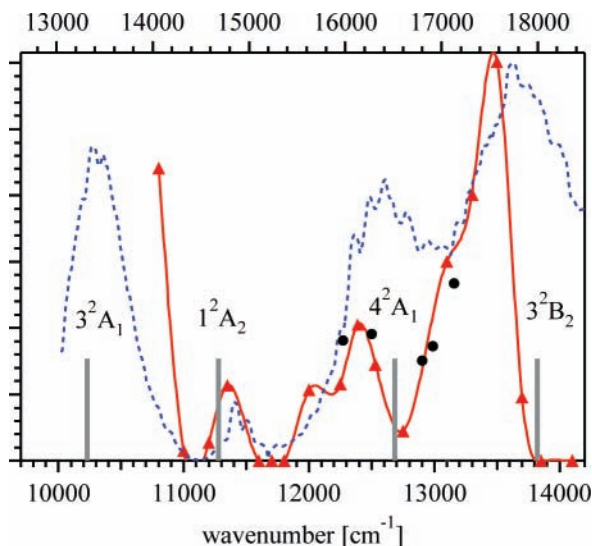
We devote the rest of this section to discussing which spin multiplicity one can expect on Ar clusters. Dissipation of molecular binding energy into the cluster environment is an issue to be considered, when looking at molecule formation on the rare-gas cluster. One has to consider the binding energy of the molecule to the cluster in relation to the binding energy of rare gas atoms to the cluster, as well as the molecular binding energy D_e, which has to be dissipated into the cluster. Dimers, specifically K$_2$ molecules, can be in either a covalently bound singlet state ($D_e \approx 4500$ cm^{-1}) or a van der Waals triplet state ($D_e \approx 200$ cm^{-1}). Alkali-metal atoms are bound to helium droplets by a few tens of cm^{-1}, and each He atom is bound by 5 cm^{-1}. Formation of a singlet dimer (and, by extension, of low-spin n-mers) releases enough energy to cause desorption from the droplet surface, whereas in the case of a triplet dimer, D_e can be dissipated by evaporation of just 40 He atoms. Thus the molecular species predominant in experiments involving helium droplets are the high-spin complexes.[12]

In Ar clusters, in contrast, each Ar atom is bound to the cluster by about 400 cm^{-1}. An immediate consequence is that argon clusters can dissipate much more energy by evaporation, and singlet dimers have a better probability of surviving desorption.

On the other hand, the cluster temperature is also competitive with dissociation of the triplet dimer. At the request of one of the referees, we estimate that the fraction of dissociated dimers at thermodynamic equilibrium at 35 K would be 0.44. The estimate is made with the statistical approach presented in chapter 10 of ref 88 (molecular data from ref 89), with the main difference that motion is restricted to the cluster surface. The degree of freedom perpendicular to the surface is accounted for by a harmonic-oscillator partition function, whose frequency was obtained from the curvature of the K−Ar$_N$ potential from MD calculation (∼8 × 10^{11} Hz, or ∼12 times the force constant of the K−Ar pair potential[65]). The calculation above does not contain the singlet K$_2$ state, which will act as a sink for atoms: based on spin multiplicity only, there is a 0.25 probability that two recombining atoms form a singlet K$_2$. We argue that after a few dissociation−recombination cycles, which should be fast compared to the time-of-flight through the experimental chamber, ∼1 ms, all dimers will end up in a singlet state. Surviving triplet dimers, if any, may be significantly distorted: On the basis of the sum of K−Ar pairwise interactions in the MD calculations, we estimate that K atoms are bound to the cluster by about 340 cm^{-1}, which for the triplet dimer means that the

Figure 10. Comparison of trimer spectral component (triangles and spline interpolation, same as Figure 5), three-photon-ionization data (circles, zero-delay signal, from ref 50), and electronic transitions from CASSCF calculations (bars, position only, no intensity information). All these data pertain to potassium and are referred to the bottom axis. A further comparison is made with scaled Na_3 data, (dotted line, digitized from ref 58), which are referred to the top axis. See text about the scaling method.

interaction with the substrate strongly competes with the interaction of the two K atoms.

Altogether, we assume that on Ar clusters one should observe mainly spectra from low-spin molecules.

In Figure 9 we show the Franck−Condon factors (FCF), convoluted with a Gaussian of arbitrary width (100 cm^{-1}), for the four lowest dipole-allowed transitions of gas-phase K_2. The FCF have been simulated at 35 K with LeRoy's Level 7.5 code,[90] and the K_2 potentials from ref 91. The resulting curves have been normalized to the same area.

C. K_3. The spectral contribution we attribute to K_3 presents the sharpest and best isolated features. Prior experimental data only exist for the high-spin (quartet) state, formed on He droplets: two bands, with bandheads at 11900 and 12700 cm^{-1} have been measured and assigned.[51,52] Due to the stronger perturbation of the Ar cluster, just the fact that these bands do not match in shape or position our measured spectrum is no strong argument to exclude this same assignment for our spectrum. For the reasons presented above, however, we are more inclined to think that low-spin (doublet) states are a better candidate.

To our knowledge, neither experimental spectra nor a calculated level structure exists for doublet K_3. The zero-delay signal measured in three-photon ionization experiments by Ruppe et al.[50] and assigned to an unspecified transition of doublet K_3 does indeed match our spectrum nicely (Figure 10). It is unfortunate that only a few data points are available and that a definite assignment is lacking.

In ref 52, Reho et al. suggest that "the energies of the excited electronic states of the alkali-metal dimers and trimers scale in an approximate way with the energy of the corresponding atomic excitations." In going from Na_3 to K_3, the scaling factor is 1.302 (Na 3s−3p and K 4s−4p atomic excitation energies from ref 63). As we verified, the calculated level structure for the lowest-energy states of the two molecules is practically the same, and in most cases there is good *qualitative* agreement. Our measured spectrum can then be compared both to CASSCF calculations and to the scaled Na_3-depletion spectrum measured by Wang

et al.,[58] as shown in Figure 10. As evident, if one accepts the scaling argument, not only the structure but also the peak intensity of our spectrum does match nicely that of Na_3. On this basis, one would assign the observed peaks as follows: 3^2A_1 (obs/calc: <11000 cm^{-1}/10230 cm^{-1}), 1^2A_2 (11350 cm^{-1}/11280 cm^{-1}), 4^2A_1 (12400 cm^{-1}/12690 cm^{-1}), 3^2B_2 (13470 cm^{-1}/13830 cm^{-1}).

Despite the good agreement between the experimental spectrum and calculated K_3 transitions, as well as scaled Na_3 data, the possibility of cluster-induced shifts has of course to be considered; thus alternative assignments should not be excluded. Besides, if part of the monomer spectrum is really due to a complex with a strongly interacting impurity such as a water molecule, the same eventuality is to be considered for K_3. We argue that alkali-metal atoms are much more strongly affected by complexation with impurities than alkali-metal molecules are, because in the latter case the impurity is competing with a strong interaction in the internuclear region; thus the presence of an impurity should not significantly affect the spectrum of K_3. We have no direct evidence that this should be the case. We note, however, that the 3S → 4S transition of Na is shifted from ≈17000 to ≈14000 cm^{-1} upon complexation with water,[92] and to ≈12000 cm^{-1} upon complexation with ammonia,[93] whereas the transition energies of Na_2 (indirectly deduced from the photoelectron spectra of Na_2^-) shift at most by 0.2 eV (∼1600 cm^{-1}) upon complexation with ammonia,[94] and those of Na_3 (also from photoelectron spectra of Na_3^-) at most by 0.06 eV (∼500 cm^{-1}).[95]

V. Summary

We have observed electronic spectra of potassium atoms, dimers, and trimers attached to argon clusters, with results whose interpretation is not straightforward.

Monomer, dimer, and trimer contributions were identified by analyzing the growth of the beam-depletion signal versus alkali-metal density in the pickup cell. The procedure relies on information obtained from a series of experiments with Rb on He droplets.

The beam-depletion spectrum we tentatively assign to the K atom is considerably broadened and contains a line doublet that is strongly red-shifted (peaks at 11220 ± 20 and 11980 ± 20 cm^{-1}, respectively) from the K atomic lines, and a weaker blue-shifted shoulder. MD simulations are unable to account for a strong red shift. Part of the spectrum may originate from a complex of K with an impurity such as H_2O.

The dimer's contribution is not further analyzed nor assigned, but we discuss reasons why we believe it should originate from singlet, rather than triplet, dimers.

For the assignment of the electronic transitions of the doublet-K_3 spectrum, CASSCF calculations for the lowest 12 states were performed. This is, to our knowledge, the first time that excited-state data are published. The level structure from the calculation was gauged against that of Na_3, suitably scaled. Experimental and computational data nicely match the Na_3 data.

Except from an unassigned fluorescent band at wavenumbers >13300 cm^{-1} no significant LIF is observed, meaning either too weak a signal or emission shifted too far to the red or nonradiative relaxation. Dispersed fluorescence of the band only shows emission from free K atoms.

12396 *J. Phys. Chem. A, Vol. 111, No. 49, 2007*

Nagl et al.

References and Notes

(1) Gough, T. E.; Mengel, M.; Rowntree, P. A.; Scoles, G. *J. Chem. Phys.* **1985**, *83*, 4958.

(2) Goyal, S.; Schutt, D. L.; Scoles, G. *J. Chem. Phys.* **1995**, *102*, 2302.

(3) Himmel, H.-J.; Downs, A. J.; Greene, T. M. *Chem. Rev.* **2002**, *102*, 4191.

(4) Almond, M.; Wilshire, K. *Annu. Rep. Prog. Chem. C* **2001**, *97*, 3.

(5) van de Waal, B. W.; Torchet, G.; de Feraudy, M.-F. *Chem. Phys. Lett.* **2000**, *331*, 57.

(6) Balling, L. C.; Wright, J. J. *J. Chem. Phys.* **1983**, *79*, 2941.

(7) Farges, J.; de Feraudy, M.-F.; Raoult, B.; Torchet, G. *Surf. Sci.* **1981**, *106*, 95.

(8) Danylchenko, O. G.; Kovalenko, S. I.; Samovarov, V. N. *Low. Temp. Phys.* **2004**, *30*, 166.

(9) Wang, C.-R.; Huang, R.-B.; Liu, Z. Y.; Zheng, L. S. *Chem. Phys. Lett.* **1994**, *227*, 103.

(10) Lewerenz, M.; Schilling, B.; Toennies, J. P. *J. Chem. Phys.* **1995**, *102*, 8191.

(11) Vongehr, S.; Kresin, V. V. *J. Chem. Phys.* **2003**, *119*, 11124.

(12) Higgins, J.; Callegari, C.; Reho, J.; Stienkemeier, F.; Ernst, W. E.; Gutowski, M.; Scoles, G. *J. Phys. Chem. A* **1998**, *102*, 4952.

(13) Nauta, K.; Miller, R. E. *Science* **1999**, *283*, 1895.

(14) Nauta, K.; Moore, D.; Miller, R. *Faraday Discuss. Chem. Soc.* **1999**, *113*, 261.

(15) Behrens, M.; Fröchtenicht, R.; Hartmann, M.; Siebers, J.; Buck, U.; Hagemeister, F. C. *J. Chem. Phys.* **1999**, *111* (6), 2436.

(16) Nauta, K.; Miller, R. E. *Science* **2000**, *287*, 293.

(17) Vach, H. *J. Chem. Phys.* **1999**, *111*, 3536.

(18) Perera, L.; Amar, F. G. *J. Chem. Phys.* **1990**, *93*, 4884.

(19) Leutwyler, S.; Bösiger, J. *Chem. Rev.* **1990**, *90*, 489.

(20) Haberland, H., Ed. *Clusters of atoms and molecules II: solvation and chemistry of free clusters, and embedded, supported, and compressed clusters*; Springer-Verlag: Berlin, New York, 1994.

(21) Crépin-Gilbert, C.; Tramer, A. *Int. Rev. Phys. Chem.* **1999**, *18*, 485.

(22) Mestdagh, J. M.; Gaveau, M. A.; Gee, C.; Sublemontier, O.; Visticot, J. P. *Int. Rev. Phys. Chem.* **1997**, *16*, 215.

(23) Gaveau, M. A.; Gloaguen, E.; Fournier, P. R.; Mestdagh, J. M. *J. Phys. Chem. A* **2005**, *109*, 9494.

(24) Buck, U. *J. Phys. Chem. A* **2002**, *106*, 10049.

(25) Farnik, M.; Nahler, N. H.; Buck, U.; Slavicek, P.; Jungwirth, P. *Chem. Phys.* **2005**, *315*, 161.

(26) Xu, M.; Bačić, Z.; Hutson, J. M. *Faraday Discuss.* **2001**, *118*, 405.

(27) Xu, M.; Bačić, Z.; Hutson, J. M. *J. Chem. Phys.* **2002**, *117*, 4777.

(28) Xu, M.; Bačić, Z.; Hutson, J. M. *J. Chem. Phys.* **2002**, *117*, 4787.

(29) Xu, M.; Jiang, H.; Bačić, Z. *J. Chem. Phys.* **2004**, *121*, 11045.

(30) Jiang, H.; Xu, M.; Hutson, J. M.; Bačić, Z. *J. Chem. Phys.* **2005**, *123*, 054305.

(31) Nauta, K.; Miller, R. E. *J. Chem. Phys.* **2001**, *115*, 10138.

(32) Stienkemeier, F.; Higgins, J.; Callegari, C.; Kanorsky, S. I.; Ernst, W. E.; Scoles, G. *Z. Phys. D: At. Mol. Clusters* **1996**, *38*, 253.

(33) Callegari, C.; Higgins, J.; Stienkemeier, F.; Scoles, G. *J. Phys. Chem. A* **1998**, *102*, 95.

(34) Weyhmann, W.; Pipkin, F. M. *Phys. Rev.* **1965**, *137*, A490.

(35) Coufal, J.; Nagel, U.; Burger, M.; Lüscher, E. *Z. Phys. B: Condens. Matter.* **1976**, *25*, 227.

(36) Schrimpf, A.; Sulzer, G.; Stöckmann, H.-J.; Ackermann, H. *Z. Phys. B: Condens. Matter.* **1987**, *67*, 531.

(37) Higgins, J. P. Helium Cluster Isolation Spectroscopy. Ph.D. thesis, Princeton University, 1998.

(38) Visticot, J. P.; de Pujo, P.; Mestdagh, J. M.; Lallement, A.; Berlande, J.; Sublemontier, O.; Meynadier, P.; Cuvellier, J. *J. Chem. Phys.* **1994**, *100*, 158.

(39) Gaveau, M. A.; Briant, M.; Fournier, P. R.; Mestdagh, J. M.; Visticot, J. P.; Calvo, F.; Baudrand, S.; Spiegelman, F. *Eur. Phys. J. D* **2002**, *21*, 1531.

(40) Gaveau, M. A.; Briant, M.; Fournier, P. R.; Mestdagh, J. M.; Visticot, J. P. *J. Chem. Phys.* **2002**, *116*, 955.

(41) Gross, M.; Spiegelmann, F. *J. Chem. Phys.* **1998**, *108*, 4148.

(42) Gervais, B.; Giglio, E.; Jacquet, E.; Ipatov, A.; Reinhard, P.-G.; Suraud, E. *J. Chem. Phys.* **2004**, *121*, 8466.

(43) Boatz, J. A.; Fajardo, M. E. *J. Chem. Phys.* **1994**, *101*, 3472.

(44) Kuppelmaier, H.; Stöckmann, H.-J.; Steinmetz, A.; Görlach, E.; Ackermann, H. *Phys. Lett.* **1983**, *98A*, 187.

(45) Kornath, A.; Zoermer, A.; Ludwig, R. *Inorg. Chem.* **1999**, *38*, 4696.

(46) Lindsay, D. M.; Herschbach, D. R.; Kwiram, A. L. *Mol. Phys.* **1976**, *32*, 1199.

(47) Mile, B.; Howard, J. A.; Histed, M.; Morris, H.; Hampson, C. A. *Faraday Discuss.* **1991**, *92*, 129.

(48) Mile, B.; Sillman, P. D.; Yacob, A. R.; Howard, J. A. *J. Chem. Soc., Dalton* **1996**, *1996*, 653.

(49) Thompson, G. A.; Lindsay, D. M. *J. Chem. Phys.* **1981**, *74*, 959.

(50) Ruppe, H.; Rutz, S.; Schreiber, E.; Wöste, L. *Chem. Phys. Lett.* **1996**, *257*, 356.

(51) Higgins, J.; Callegari, C.; Reho, J.; Stienkemeier, F.; Ernst, W. E.; Lehmann, K. K.; Scoles, G. *Science* **1996**, *273*, 629.

(52) Reho, J. H.; Higgins, J.; Nooijen, M.; Lehmann, K. K.; Scoles, G.; Gutowski, M. *J. Chem. Phys.* **2001**, *115*, 10265.

(53) Broyer, M.; Delacretaz, G.; Labastie, P.; Wolf, J. P.; Wöste, L. *Phys. Rev. Lett.* **1986**, *57*, 1851.

(54) Ernst, W. E.; Rakowsky, S. *Can. J. Phys.* **1994**, *72*, 1307.

(55) Ernst, W. E.; Rakowsky, S. *Phys. Rev. Lett.* **1995**, *74*, 58.

(56) Vituccio, D. T.; Golonzka, O.; Ernst, W. E. *J. Mol. Spectrosc.* **1997**, *184*, 237.

(57) Broyer, M.; Delacrétaz, G.; Labastie, P.; Whetten, R. L.; Wolf, J. P.; Wöste, L. *Z. Phys. D: At. Mol. Clusters* **1986**, *3*, 131.

(58) Wang, C. R.; Pollack, S.; Cameron, D.; Kappes, M. M. *J. Chem. Phys.* **1990**, *93*, 3787.

(59) Cocchini, F.; Upton, T. H.; Andreoni, W. *J. Chem. Phys.* **1988**, *88*, 6068.

(60) Goyal, S. On the Size Dependence of the Infrared Spectrum of SF_6 in and on Noble Gas Clusters: Finite Size Particles Attaining Bulk-like Properties. Ph.D. thesis, Princeton University, 1992.

(61) Lide, D. R. Ed. *CRC Handbook of Chemistry and Physics*, 77th ed.; CRC Press: Boca Raton, FL, 1996−97.

(62) Stienkemeier, F.; Wewer, M.; Meier, F.; Lutz, H. O. *Rev. Sci. Instrum.* **2000**, *71*, 3480.

(63) Ralchenko, Y.; Jou, F.-C.; Kelleher, D. E.; Kramida, A. E.; Musgrove, A.; Reader, J.; Wiese, W. L.; Olsen, K. *NIST atomic spectra database* Version 3.1.1; National Institute of Standards and Technology: Gaithersburg, MD, 2007; http://physics.nist.gov/PhysRefData/ASD/index.html.

(64) Rossi, F.; Pascale, J. *Phys. Rev. A* **1985**, *32*, 2657.

(65) Bokelmann, F.; Zimmermann, D. *J. Chem. Phys.* **1996**, *104*, 923.

(66) Pauly, H. *Molecular beams and methods*; Oxford: New York, 1988; Vol. 1, Chapter 4.

(67) Berendsen, H. J. C.; Postma, J. P. M.; van Gunsteren, W. F.; DiNola, A.; Haak, J. R. *J. Chem. Phys.* **1984**, *81*, 3684.

(68) Morishita, T. *Mol. Simul.* **2003**, *29*, 63.

(69) Podeszwa, R.; Szalewicz, K. *Chem. Phys. Lett.* **2005**, *412*, 488.

(70) El Hadj Rhouma, M. B.; Berriche, H.; Lakhdar, Z. B.; Spiegelman, F. *J. Chem. Phys.* **2002**, *116*, 1839.

(71) Spiegelman, F.; Maron, L.; Breckenridge, W. H.; Mestdagh, J.-M.; Visticot, J. P. *J. Chem. Phys.* **2002**, *117*, 7534.

(72) Czuchaj, E.; Rebentrost, F.; Stoll, H.; Preuss, H. *Theor. Chem. Acc.* **1998**, *100*, 117.

(73) Figl, C.; Grosser, J.; Hoffmann, O.; Rebentrost, F. *J. Phys. B At. Mol. Opt.* **2004**, *37*, 3369.

(74) Gaus, J. Strukturelle und elektronische Eigenschaften kleiner reiner, gemischter und dotierter Alkalimetall-Cluster. Doctoral thesis, Freie Universität Berlin, 1995.

(75) Martins, J. L.; Car, R.; Buttet, J. *J. Chem. Phys.* **1983**, *78*, 5646.

(76) Spiegelmann, F.; Pavolini, D. *J. Chem. Phys.* **1988**, *89*, 4954.

(77) Werner, H.-J.; Meyer, W. *J. Chem. Phys.* **1980**, *73* (5), 2342.

(78) Werner, H.-J.; Meyer, W. *J. Chem. Phys.* **1981**, *74*, 5794.

(79) Werner, H.-J.; Knowles, P. J. *J. Chem. Phys.* **1985**, *82*, 5053.

(80) Knowles, P. J.; Werner, H.-J. *Chem. Phys. Lett.* **1985**, *115*, 259.

(81) Werner, H.-J.; Knowles, P. J.; Lindh, R.; Manby, F. R.; Schütz, M.; Celani, P.; Korona, T.; Rauhut, G.; Amos, R. D.; Bernhardsson, A.; Berning, A.; Cooper, D. L.; Deegan, M. J. O.; Dobbyn, A. J.; Eckert, F.; Hampel, C.; Hetzer, G.; Lloyd, A. W.; McNicholas, S. J.; Meyer, W.; Mura, M. E.; Nicklass, A.; Palmieri, P.; Pitzer, R.; Schumann, U.; Stoll, H.; Stone, A. J.; Tarroni, R.; Thorsteinsson, T. Molpro, version 2006.1, a package of ab initio programs. 2006.

(82) Lim, I. S.; Schwerdtfeger, P.; Metz, B.; Stoll, H. *J. Chem. Phys.* **2005**, *122*, 104103.

(83) Derevianko, A.; Johnson, W. R.; Safronova, M. S.; Babb, J. F. *Phys. Rev. Lett.* **1999**, *82*, 3589.

(84) Amiot, C. *J. Mol. Spectrosc.* **1991**, *147*, 370.

(85) Boys, S. F.; Bernardi, F. *Mol. Phys.* **1970**, *19*, 553.

(86) Werner, H.-J. *Mol. Phys.* **1996**, *89*, 645.

(87) Reho, J.; Callegari, C.; Higgins, J.; Ernst, W. E.; Lehmann, K. K.; Scoles, G. *Faraday Discuss.* **1997**, *108*, 161.

(88) Hill, T. L. *An Introduction to Statistical Thermodynamics*, 2nd ed.; Dover Publications: New York, 1986.

(89) Ahmed, E.; Lyyra, A.; Xie, F.; Li, D.; Chu, Y.; Li, L.; Ivanov, V.; Sovkov, V.; Magnier, S. *J. Mol. Spectrosc.* **2005**, *234*, 41.

(90) Le Roy, R. J. LEVEL 7.5. a computer program for solving the radial Schrödinger equation for bound and quasibound levels Chemical Physics Research Report CP-655, University of Waterloo, Canada, 2002.

(91) Magnier, S.; Aubert-Frécon, M.; Allouche, A. R. *J. Chem. Phys.* **2004**, *121*, 1771.

Optical Spectroscopy of Potassium-Doped Ar Clusters

J. Phys. Chem. A, Vol. 111, No. 49, 2007 **12397**

(92) Schulz, C. P.; Bobbert, C.; Shimosato, T.; Daigoku, K.; Miura, N.; Hashimoto, K. *J. Chem. Phys.* **2003**, *119* (22), 11620.

(93) Brockhaus, P.; Hertel, I. V.; Schulz, C. P. *J. Chem. Phys.* **1999**, *110* (1), 393.

(94) Takasu, R.; Hashimoto, K.; Okuda, R.; Fuke, K. *J. Phys. Chem. A* **1999**, *103*, 349.

(95) Fujihara, A.; Miyata, C.; Fuke, K. *Chem. Phys. Lett.* **2005**, *411*, 345.

(96) N_2 gas was resistively evaporated from a reservoir of liquid, which we found to give better thermal and mechanical stability as compared to direct cooling with liquid N_2. Altogether, we found it more difficult to thermally stabilize the system with N_2 than with He, probably because of the large heating/cooling powers involved.